chemosensors

MDPI

Article

Selectivity and Efficiency of Conductive Molecularly Imprinted Polymer (c-MIP) Based on 5-Phenyl-Dipyrromethane and 5-Phenol-Dipyrromethane for Quorum Sensing Precursors Detection

Sabina Susmel * and Clara Comuzzi

Department of Agricultural, Food, Environmental and Animal Sciences (Di4A), University of Udine, Via delle Scienze 208, 33100 Udine, Italy; Clara.Comuzzi@uniud.it

* Correspondence: Sabina.Susmel@uniud.it; Tel.: +39-432-558-823

Academic Editor: Peter Lieberzeit

Received: 3 December 2016; Accepted: 27 January 2017; Published: 4 February 2017

Abstract: Functional polymers that selectively recognize target compounds are developed by imprinting polymerization. In the present paper, two different dipyrromethanes, 5-phenol-dipyrromethane (5-pOH-DP) and 5-phenyl-dipyrromethane (5-ph-DP), are synthetized and investigated to develop conductive molecularly imprinted polymer (cMIP) sensors. As target molecules, two homoserine lactone derivatives were templated by an electrochemically driven polymerization process. Acyl-homoserine lactones (AHLs), also called homoserine lactones (HS), are a class of signaling molecules involved in bacterial *quorum sensing* (QS), which is a strategy of coordination among bacteria mediated by population density. The preparation of cMIP from 5-pOH-DP and 5-ph-DP in the presence of acetyl-homoserine lactone (Acetyl-HS) or carboxybenzyl-homoserine lactone (Cbz-HS) was performed by cyclic voltammetry (CV). The cMIP selectivity and sensitivity were assessed by microgravimetry (QCM). Both series of measurements were performed with the aid of an Electrochemical Quartz Crystal Microbalance (EQCM/QCM). The experimental evidences are discussed with respect to NMR measurements that were conducted to gain insight into the interactions established between monomers and templates. The NMR data interpretation offers preliminary information about the most probable positions involved in interaction development for both molecules and highlights the role of the hydration shell. The QCM-cMIP sensor was able to detect the analyte in the linear range from 10^{-8} mol·L^{-1} to 10^{-6} mol·L^{-1} and a limit of detection (LOD) of 22.3 ng (3σ of the blank signal) were evaluated. QCM rebinding tests demonstrated that cMIP selectivity was driven by the pendant group of dipyrromethane, which was also confirmed by the NMR data.

Keywords: 5-phenol-dipyrromethane; 5-phenyl-dipyrromethane; electrochemical polymerization; molecularly imprinted polymer; quorum sensing; ESQCM/QCM; NMR

1. Introduction

The development of sensors based on molecular imprinted polymers (MIPs) has received great attention in recent years [1–3]. The preparation of MIP is based on the ability to create a "fingerprint" into the polymerizing matrix by the template molecule. Once the template molecule is removed from the polymer, the generated cavity, which is defined by its size and stereochemical configuration, acts as a 3D recognition unit that is highly specific for the target analyte [4,5]. Five main types of molecular imprinting techniques are described, i.e., noncovalent, electrostatic/ionic, covalent,

semicovalent, and coordination at the metal centers [6,7]. The difference among these approaches is related to the strategy adopted to stabilize the template to the monomer during the polymerization step. In this process, it is essential that the template interacting with the monomer does not deactivate the polymerization positions. The very high versatility offered by the chemical polymerization strategy [8–10] is difficult to transfer to polymerization that is electrochemically driven, as the availability of an electroactive monomer is introduced as a constraint. Pyrrole or (di)-thiophene are frequently used for conductive MIP preparation [11–15]. For this particular imprinting approach, the template stabilization and inclusion uses a non-covalent strategy, which is based on the charge interaction between the electrogenerated aromatic cation and the template in ionic form [12,15]. Thus, the process is limited and can lack selectivity [14,16]. To respond to these drawbacks and to enlarge the fields of application, "bifunctional" monomers, whose structures bear both the unit devoted to the molecular recognition and the unit of polymerization, were applied. However, in most cases, the functionalization of the monomer impairs its polymerization features, and thus some molecular structures can solely be used as recognition moiety [17,18]. Consequently, the selectivity cannot be accurately tuned, given that it is generally argued that imprinted polymers cannot match the affinities offered by natural receptor sites. The reasons are twofold: first, the entropic contribution for selective recognition due to the shape of the cavity is not sufficient because the specific short-range interactions that exist in the natural binding sites generally do not exist in the imprints; second, as the polymerization is performed in solution, the template and monomer are both solvated. The solvation shell contributes in a significant way to the overall shape and size of the template and it can be modified during the polymerization or rebinding step [19]. In the rebinding process, the solvation of the 3D imprinted cavity modulates the interactions with the template [20]. Recently, however, some important advances in affinity and specificity of soluble imprinted nano-polymers have been reported [8–10].

The aim of the present paper is to investigate new electroactive bifunctional molecules for imprinting processes and the role of the molecular features in driving the affinity interactions in these synthetic receptors. In our previous work [21], we demonstrated that dipyrromentanes (Figure 1) are useful monomers to synthesize electrochemically conductive MIP (cMIP). In particular, we customized an efficient and selective sensor for salicylic acid using dipyrromethanes whose different substitution in C5 ensured both π–π interactions and hydrogen bonding. The present work represents a further step in demonstrating our original idea that dipyrromethanes can serve as amino acid-like monomers to build receptor-like cMIP.

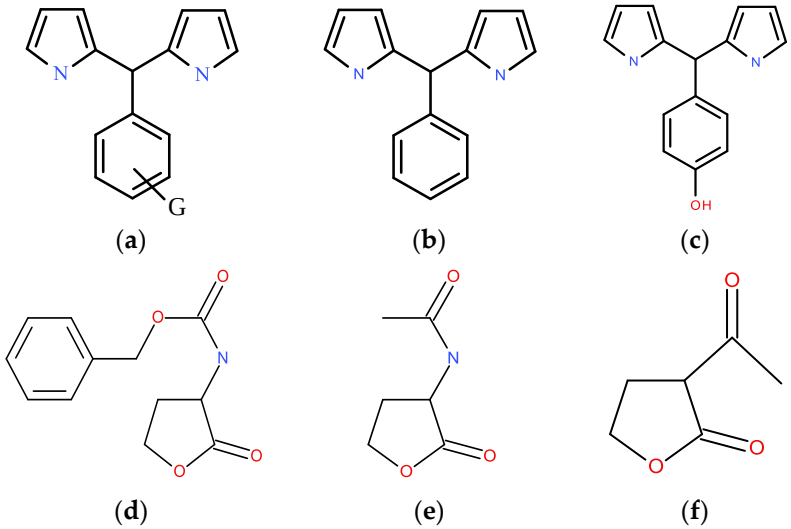

Figure 1. (**a**) General formula of 5-substituted dipyrromethanes; (**b**) 5-phenyl dipyrromethane; (**c**) 5-phenol dipyrromethane; (**d**) N-carbobenzoxy-L-homoserine Lactone (Cbz-HS) used as template; (**e**) acetyl-HS used as template; (**f**) α-acetyl-butyrolactone used as interferent.

The binding pocket of the receptor QscR (*Q*uorum-*s*ensing *c*ontrol *r*epressor) of *P. Aeruginosa* has been chosen to test our assumptions. QscR is an additional LuxR homolog in *P. Aeruginosa* which responds to acyl-homoserine lactone (AHLs), the *quorum sensing* signal controlling gene expression in Gram-bacteria. Recently, the crystal structure of QscR bound to 3-oxo-dodecanoyl-homoserine lactone [22] has been determined, showing numerous hydrogen bonds between the receptor cavity and the acyl-homoserine lactone derivative. According to the reported structure, the carbonyl group of homoserine lactone is bound to a tryptophan residue, the carbonyl group of the acyl chain is bound to the phenolic hydroxylic group of a tyrosine residue, and the -NH of the AHL is bound to the carboxylate moiety of an asparagine residue (see Supplementary Materials, Figure S1). These interactions are generally conserved in all AHL receptors. Gram-negative (G-) bacteria produce AHLs differing in the acyl chain structure, thus the response specificity of the AHL receptors is driven by the acyl-chain binding pocket where amino acidic residues such as phenylalanine, leucine, and valine are found. The QscR-AHL structure described above was taken as a reference for synthesizing a cMIP sensor for AHL based on dipyrromethanes. Due to the complexity of the system and the need to gain insight about the role of the individual monomers in the interaction with the template, we chose to use only two monomers. Inspired by the QscR bio-receptor acyl chain binding pocket, 5-phenol-dipyrromethane (5-pOH-DP) was selected as an analogue of tyrosine and 5-phenyl-dipyrromethane (5-ph-DP) as an analogue of phenylalanine. Two homoserine lactone derivatives, (*N*-carbobenzoxy-L-homoserine Lactone (Cbz-HS) and *N*-Acetyl-L-homoserine lactone (Acetyl-HS)) (Figure 1), were selected as templates to investigate the interaction and selectivity ability of the two dipyrromethanes towards changes in the acylic tail.

Structural biology prompted NMR spectroscopy towards the development of methods to elucidate the structure, interaction, and dynamics of molecules in solution [23]. When two molecules interact with each other, the variation of the electronic environment at the sites involved in the bond causes detectable changes in NMR chemical shifts, line shapes, and relaxation rates. Preliminary NMR measurements were thus conducted to shed light on the interactions between monomers and templates in solution.

The electrochemical behavior of the monomers and their polymerization ability through the registration of the simultaneous signal of current and mass variation was investigated by cyclic voltammetry (CV) at a Pt-quartz crystal electrode with an EQCM (Electrochemical Quartz Crystal Microbalance) potentiostat. The analytical performances of cMIP were characterized by QCM (Quartz Crystal Microbalance) and a microgravimetric signal variation was recorded. The cMIP were obtained with both monomers and different uptakes were measured, with poly-5-pOH-DP found to be more efficient than poly-5-ph-DP in hosting the templates.

NMR data confirmed that 5-ph-DP interacted weakly with the template and preferentially at the phenyl-ring and on pyrrolic units. 5-pOH-DP developed a stronger interaction with the templates than 5-ph-DP mainly through H bonding at the phenolic OH group and at the template's amide NH group. This evidence was in agreement with the electrochemical data as a positive shift of potential (Ep) and a higher oxidation peak current (i_p) was measured due to the perturbation of the inductive effect of phenolic-OH caused by the interaction with the template. Moreover, in cMIP poly-5-pOH-DP, the network of H bonding developed during polymerization imposed an impressive interaction selectivity towards interfering molecules. It was demonstrated that a 3D cavity, with a high level of fitting, tuned by the pendant group of dipyrromethanes, was prepared.

2. Materials and Methods

2.1. Materials

All reagents and solvents were obtained from Sigma-Aldrich (Milan, Italy), if otherwise stated, and were of the highest purity commercially available. They were utilized as received.

2.2. Instrumentations and Procedures

Thin Layer Chromatography (TLC) analysis was conducted on TLC plastic sheets 60 F254 (Fluka-Sigma-Aldrich, Milan, Italy) with detection by UV absorption. Column chromatography was performed using silica gel (0.063–0.200 mm particle size, 70–230 mesh) purchased from Merck. 1H-NMR spectra were acquired with a Bruker 200 NMR spectrometer (200 MHz). Stock solutions (50 mM) of 5-pOH-DP, 5-ph-DP, *N*-acetyl homoserine lactone, and *N*-carbobenzoxy-L-homoserine lactone were prepared in acetonitrile-d3. Aliquots of stock solutions were withdrawn and diluted with acetonitrile-d3 to obtain 10 mM solutions. 1H-NMR sample of 5-pOH-DP, 5-ph-DP, Cbz-HS, and Acetyl-HS and of 1:1 mixtures (10 mM in each components) of 5-pOH-DP/Cbz-HS, 5-pOH-DP/Acetyl-HS, 5-ph-DP/Cbz-HS, and 5-ph-DP/Acetyl-HS were prepared.

Chemical shifts are reported in ppm with tetramethylsilane (TMS) as an internal reference. The abbreviations used are: s = singlet, d = doublet, dd = doublet of doublets, m = multiplet, and br = broad. The probe temperature was calibrated using methanol by the method of Van Geet [24]. Temperature coefficients were estimated by the standard method using chemical shift data from four temperatures in the range of 233–298 K. IR spectra were recorded with an FT-IR from Bruker model Vector 22 equipped with Attenuated Total Reflectance (ATR) crystal.

A Time-resolved Electrochemical Quartz Crystal Microbalance (EQCM) potentiostat/galvanostat CHI 400C (CH Instruments, Inc., Austin, TX, USA) working station was used to carry out the measurements. This potentiostat has access to electroanalytical or microgravimetric or combined electromicrogravimetric determinations when used either in EQCM or in QCM mode. The potentiostat interfaced with a computer with the CHI 16.03 software version control. The electrochemical measurements were performed using three electrodes in a one-compartment static Teflon cell, sealed with a Teflon cap to avoid solvent evaporation. The voltage was applied at the Pt-quartz crystal working electrode (WE), with respect to an Ag/Ag^+ non-aqueous reference electrode (RE) and a Pt-wire auxiliary electrode (AE). All instrumentation, software, and accessories were from CH Instruments, Inc., Austin, TX, USA. In EQCM operative mode, the current variation (i_p) in relation with the applied potential at the Pt-quartz WE was recorded. When needed, the i_p was recorded together with the frequency shift (Δf in Hz) due to the mass variation at the quartz crystal surface. Δf due to the mass variation at the Pt-quartz crystal surface was recorded, instead, as a single signal in microgravimetric (QCM) mode. Quartz crystal microbalance (QCM) data were analyzed according to the Saurebrey equation [25].

$$\Delta f = -2{f_0}^2 \, \Delta m / [A \, (\mu \, \rho)^{1/2}]$$

where Δf has the reported meaning, f_0 is the fundamental oscillation frequency of the dry crystal, Δm (g) is the surface mass loading, A is the electrode area, ρ is the density of the crystal, and μ is the shear modulus. The characteristics of the Pt-quartz crystal used were: AT-cut, f_0 = 8 MHz, density (ρ) 2.684 g/cm^3, shear modulus of quartz (μ) 2.947 $\times$ 10^{11} g/cm·s^2, electrode area (A) 0.196 cm^2. Therefore, a frequency shift of 1 Hz corresponds to a mass increase of 1.34 ng on the electrode. Each crystal was used several times and was polished by sonication following this protocol: 2 min in acetone, 2 min in acetonitrile (AN) with 50% of water solution of NaOH 0.1 M (prepared in ultrapure water) added, 2 min in AN with 1% of Acetic acid (HAc) added, and finally 2 min in acetone. It was gently dried under a flow of air.

2.3. Synthesis of 5-Phenyl-Dipyrromethane (5-ph-DP)

5-phenyl-dipyrromethane (5-ph-DP) was synthesized as reported in the literature [26–28]. Briefly, pyrrole (7 mL) and benzaldehyde (0.4 mL) were degassed with N_2 for 15 min. A volume of 0.03 mL of trifluoroacetic acid (TFA) was then added and the reaction mixture was stirred for 15 min. Evaporation to dryness and flash chromatography (Petroleum Ether/Ethyl Acetate 95/5) produced 5-ph-DP with a 61% yield.

1H-NMR (acetonitrile-d3) δ (ppm) 5.41 (s, 1H), 5.75 (m, 2H), 5.98 (m, 2H), 6.62 (m, 2H), 7.19 (d, 5H), 8.9 (br s, NH).

FTIR-ATR powder 3368 (ν NH), 3343 (ν NH), 1554 (ν aromatic C=C), 1113 and 1025 (δ N-H, δ C-H), 739, 724, 714, 702, 594, 583, 502 cm^{-1} [29].

2.4. Synthesis and Characterization of 5-Phenol-Dipyrromethane (5-pOH-DP)

A volume of 3 mL of pyrrole and 500 mg of 4-hydroxybenzaldehyde were degassed with N_2 for 15 min. The reaction mixture was cooled to 0 °C and then 0.25 mL of trifluoroacetic acid (TFA) was added dropwise under nitrogen flux. When the acid addition was completed, the reaction was allowed to continue for 30 min at 0 °C, followed by 45 min at room temperature. The reaction was then cooled with an ice bath and 2 mL of $NaHCO_3$ 5% was added and diluted with Ethyl Acetate (EtOAc). The organic phase was separated, dried over Na_2SO_4, and evaporated with N_2.

The thick oil obtained was purified by flash chromatography on silica (Petroleum ether/Ethyl Acetate 85/15) producing pure 5-pOH-DP with a 30% yield.

1H-NMR (acetonitrile-d3) δ (ppm) 5.32 (s, 1H), 5.73 (m, 2H), 5.96 (m, 2H), 6.60 (m, 2H), 6.71 (d, 2H), 7.05 (d, 2H), 8.82 (br s, NH).

FTIR-ATR powder 3441(ν NH), 3415(ν NH), 3357(ν OH), 1512(ν aromatic C=C), 1260 (ν C-O), 1195 and 1171 (δ N-H, δ C-H), 734, 528 cm^{-1} [29].

2.5. Synthesis and Characterisation of N-Acetyl Homoserine Lactone

N-carbobenzoxy-L-homoserine lactone (250 mg), 37.5 mg of Pd/C catalyst, and 15 mL of freshly distilled acetic anhydride were placed in a three-neck round bottom flask connected to an inert gas line, a vacuum line, and a balloon filled with hydrogen, respectively. The reaction mixture was placed under a hydrogen atmosphere, after pre-treatment with vacuum/inert gas and vacuum/hydrogen cycles, and was allowed to stand for 24 h under stirring. The mixture was then filtered and evaporated to dryness to produce *N*-acetyl-L-homoserine lactone quantitatively.

1H-NMR (acetonitrile-d3; −20 °C) NMR (200 MHz) δ 6.90 (s, NH), 4.35 (m, 3H), 2.42 (m, 1H), 2.15 (m, 1H), 1.88 (s, 3H).

2.6. Electrochemical Investigations of 5-ph-DP, 5-pOH-DP, and Homoserine Lactone Derivatives

The above described instrumentation was used to study the electrochemical behavior of 5-ph-DP and 5-pOH-DP (1×10^{-3} mol·L^{-1}), and homoserine lactone derivatives (Acetyl-HS and Cbz-HS) by cyclic voltammetry (CV). CV was performed in acetonitrile (AN) with 0.05 mol·L^{-1} of tetrabutylammonium perchlorate (TBAP) added. This solvent/electrolyte system was adopted in all measurements unless otherwise stated.

2.7. Electromicrogravimeric (EQCM) Preparation of cNIP and cMIP

The instrumentation described in Section 2.2 was used to prepare both conductive non-imprinted polymer (cNIP) and conductive molecularly imprinted polymer (cMIP). The electrochemical polymerization at the Pt-quartz-crystal by EQCM was obtained by cyclic voltammetry in the voltage range from −0.8 V and +1.2 V and 12 sweeps were used with a scan rate of 50 mVs^{-1}. cNIP was obtained from the polymerization, electrochemically driven, of either 5-ph-DP or 5-pOH-DP in solvent/electrolyte solution with no added template. To prepare cMIP, the template, Cbz-HS or Acetyl-HS, was added to the solution together with the monomer before starting the electrochemical polymerization.

After electropolymerization, the template removal from the imprinted polymer was obtained with AN + 0.05 mol·L^{-1} TBAP + 10% (*v*/*v*) HAc (30 min at RT). The extraction was performed at room temperature, in static conditions, and the washing solution was replaced every 5–6 min. A mass release (positive Δf measured) equivalent to the mass uptake and the stability in signal variation ($\Delta Hz/\Delta t = \pm 1$ Hz min^{-1}) were indicative of the extraction that occurred. Other washing solutions

tested, such as (i) AN + 0.05 mol·L^{-1} TBAP + 1% (v/v) HAc (30 min at RT); and (ii) AN + 1% (v/v) HAc + 40% (v/v) methanol (30 min at RT) were less effective.

2.8. Gravimetric (QCM) Evaluation of cMIP Sensor Performances

To evaluate the cMIP sensor response, the rebinding tests were performed by gravimetric measurement after the extraction of the template. Pt-quartz crystal modified by cMIP was submerged with 3 mL of a quiescent solution of AN/electrolyte and the analyte was added in a range of concentration from 4 × 10^{-8} mol·L^{-1} (1 × 10^{-10} mol) to 2 × 10^{-6} mol·L^{-1} (6 × 10^{-9} mol). The calibration curve was obtained from the mass shift (Δm/ng) vs. homoserine lactone concentration. Cbz-HS, Acetyl-HS, and α-acetylbutyrolactone (Figure 1) were tested as interfering compounds to evaluate the response selectivity. To evaluate the aspecific signal of cNIP, these tests were performed as well.

3. Results and Discussion

3.1. NMR Data

Our main goal was to investigate how the substituent in C5 affects the coordination ability of dipyrromethanes towards the templates and, in particular, how the phenolic OH is engaged in the bond with the homoserine derivatives. To detect the formation and the strength of hydrogen bonds, 1H-NMR chemical shift changes and temperature coefficient experiments were performed. 1H-NMR spectra of 5-pOH-DP, 5-ph-DP, Cbz-HS, and Acetyl-HS and of 5-pOH-DP/Cbz-HS, 5-pOH-DP/Acetyl-HS, 5-ph-DP/Cbz-HS, and 5-ph-DP/Acetyl-HS were recorded at intervals of 20 K over the temperature range from 233 to 293 K. All proton temperature coefficients were estimated by plotting the linear relationship of the proton chemical shift as a function of temperature. The formation of a hydrogen bond generally causes a pronounced change in resonance frequency of the bounded proton. In Table 1, changes in chemical shift ($\Delta\delta$) at 293 K are reported. The NMR sample 5-pOH-DP/Acetyl-HS registered the higher chemical shift changes. The presence of the Acetyl-HS de-shielded the phenolic OH proton, shifting the signal of 0.07 ppm compared to free 5-pOH-DP. At the same time, a de-shielding of 0.09 ppm was observed for the amide NH of Acetyl-HS compared to its free form. Additionally, the pyrrolic NH slightly moved to a higher frequency $\Delta\delta$ = 0.03 ppm). All the other signals (pyrrolic protons, the dipyrromethanic meso proton, the lactonic protons, as well as the CH_3 of Acetyl-HS) did not shift ($\Delta\delta$ = 0 ppm). These data suggest that 5-pOH-DP and Acetyl-HS interact with each other through those molecular sites capable of hydrogen bonding. The small shifts suggest also that the interaction is probably mediated by the water present in the sample. The NMR sample 5-pOH-DP/Cbz-HS showed a slight perturbation (0.03 ppm) at the -OH group together with a very small and negative $\Delta\delta$ (-0.01 ppm) of NH Cbz-HS, suggesting their weak interaction. The chemical shift changes of the 5-ph-DP samples showed that the molecule interacted very weakly with the lactone derivatives. The sample 5-ph-DP/Cbz-HS showed a slight perturbation of the proton signals of the dipyrromethane unit with $\Delta\delta = -0.01$ ppm. In any case, differences in chemical shifts ($\Delta\delta$) are difficult to interpret as they depend on many influences, i.e., the presence of nearby aromatic groups and the different degree of solvation between the free molecules and the complexes. In the case presented here, the water interactions with the studied molecules influenced their chemical shifts. The complex formation also modified the solvation shell to different extents, having a shielding effect on the chemical shift, and in the meantime, a de-shielding effect was also observed as a consequence of the complex formation itself. So, the final $\Delta\delta$ values are a result of these opposing effects and they can be difficult to interpret. Therefore, the study of H bonding is, in general, associated to the temperature coefficient determination as the H bond chemical shift is sensitive to temperature changes. The rise of temperature causes a weakening of the hydrogen bond and a shift to lower frequencies of the proton involved in the bonding. Structural studies on proteins have revealed that the lengthening of the H bond with temperature is greater for intermolecular H bonding than for internal hydrogen bonds, and

hence amide that is H bonded to water will shift more with temperature than internally H bonded amides. The so-called temperature coefficient ($\Delta\delta/\Delta T$) measures the temperature dependence of a proton involved in an H bond [30–32].

Table 1. Chemical shift changes of the NMR solution of monomers and HS-derivatives with respect to their free form.

NMR Sample Solution	Δδ (ppm)			
	$NH_{Cbz\text{-}HS}$	$NH_{Acetyl\text{-}HS}$	NH_{py}	OH_{phenol}
5-pOH-DP/Cbz-HS	−0.01		0.01	0.03
5-pOH-DP/Acetyl-HS		0.09	0.03	0.07
5-ph-DP/Cbz-HS	−0.01		−0.03	
5-ph-DP/Acetyl-HS		0.03	0.01	

Recently, temperature coefficients of phenolic OH protons were measured in different solvents [33], showing that in AN-d3, -OH protons exposed to the solvent had $\Delta\delta/\Delta T$ values in the range of −5 to −10 ppb·K^{-1}. In Table 2, $\Delta\delta/K$ values are reported for all the NMR samples. $\Delta\delta/K$ of the OH group of 5-pOH-DP was found to be −6.4 ppb·K^{-1}, in very good agreement with the literature data. The amide NH of Acetyl-HS showed a $\Delta\delta/K$ of −3.1 ppb·K^{-1}. When 5-pOH-DP and Acetyl-HS were mixed together, the temperature coefficient of its amide NH changed to −1.6 ppb·K^{-1}, indicating that the proton was involved in stronger H bonding than in free Acetyl-HS. At the same time, the $\Delta\delta/K$ of the OH group of 5-pOH-DP changed to −5.8 ppb·K^{-1}. In the 5-pOH-DP/Acetyl-HS system, both chemical shift changes and temperature coefficients showed a detectable interaction of the two molecules through the H bonding network. The temperature coefficients of 5-pOH-DP/Cbz-HS, 5-ph-DP/Cbz-HS, and 5-ph-DP/Acetyl-HS were similar to the corresponding values of the free molecules, indicating that the interaction was not driven by H bonding.

Table 2. Temperature coefficients of NMR solution of dipyrromethanes and HS-derivatives in their free form and in their mixture.

NMR Sample Solution	Δδ/K (ppb/K)			
	NH_{py}	OH_{phenol}	$NH_{Acetyl\text{-}HS}$	$NH_{Cbz\text{-}HS}$
Acetyl-HS			−3.1 (±0.1)	
Cbz-HS				−2.8 (±0.2)
5-pOH-DP	−3.0 (±0.1)	−6.4 (±0.2)		
5-ph-DP	−2.6 (±0.1)			
5-pOH-DP/Acetyl-HS	−2.7 (±0.2)	−5.8 (±0.1)	−1.6 (±0.2)	
5-ph-DP/Acetyl-HS	−2.6 (±0.3)		−2.8 (±0.1)	
5-pOH-DP/Cbz-HS	−2.9 (±0.2)	−6.2 (±0.1)		−2.9 (±0.3)
5-ph-DP/Cbz-HS	−2.9 (±0.2)			−2.8 (±0.1)

3.2. Electrochemistry of 5-ph-DP and 5-pOH-DP and Homoserine Lactone Derivatives in Solution

The structures of 5-ph-DP and 5-pOH-DP and their cyclovoltammograms recorded at the Pt-quartz crystal electrode are compared in Figure 2. The potential of the anodic peak (Ep_a) related to the formation of the radical cation was observed for 5-pOH-DP at a slightly reduced potential (+0.81 V) compared to that of 5-ph-DP observed at +0.87 V. The weaker electron donating character of the phenyl substituent in C5 compared to that of the phenol derivative was considered to affect the potential of radical cation generation at the dipyrromethane moiety. It is worth noting that the 1H-NMR spectrum of 5-pOH-DP had all signals upfield shifted compared to 5-ph-DP, demonstrating the positive inductive effect of the phenolic moiety in C5.

The investigation of the scan rate effect (data not shown) in the range from 10 to 200 mVs^{-1}, confirmed that this oxidation process for both monomers was not reversible. The investigation confirmed, as well, that the phenol pendant group was not involved in this first oxidation process as

its oxidation was evident at higher Ep (+2.5 V) [a paper discussing the electrochemistry of differently substituted dipyrromethanes is in preparation]. The FTIR of poly-5-pOH-DP showed the C-O stretching band at 1276 cm^{-1}. The electroactivity of homoserine lactone derivatives was investigated by cyclic voltammetry (Figure 3) to an anodic limit of potential of 2.7 V. An oxidation process of Cbz-HS 1 mM in a solution of acetonitrile/0.05 M TBAP, was observed at Ep = 2.1 V. The different electron-withdrawing properties of Cbz- and Acetyl-groups was seen to affect the peak shape and the oxidation potential of HS derivatives. Acetyl-HS oxidation shifted to a more positive Ep (2.4 V) as hump-like peak whose current density was increasing with the concertation.

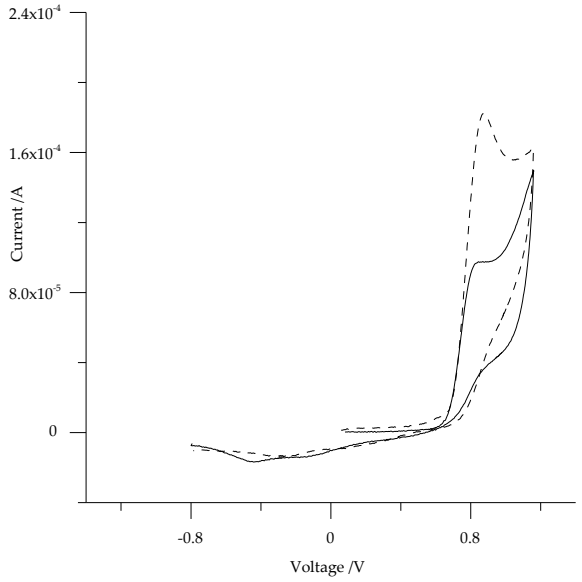

Figure 2. Cyclovoltamogram of 5-ph-DP (dashed line) and 5-pOH-DP (solid line). Monomers were separately investigated at a concentration of 1 mM in AN/0.05 M TBAP. Pt-quartz crystal WE, Ag/Ag^{+} non-aqueous RE, Pt-wire AE, scan rate 50 mVs^{-1}.

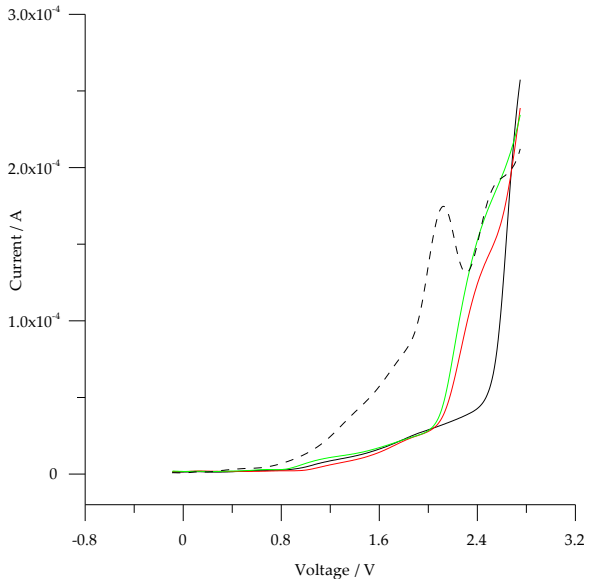

Figure 3. Anodic scan of HS-derivatives separately investigated in AN/0.05 M TBAP at the Pt-quartz crystal WE, Ag/Ag^{+} non-aqueous RE, Pt-wire AE, scan rate 50 mVs^{-1}. Cbz-HS 1 mM (dashed line); Acetyl-HS 1 mM (solid line red) and Acetyl-HS 2 mM (solid line green); solid line black: background AN/0.05 M TBAP.

Homoserine derivatives were analysed by CV in the presence of either 5-ph-DP or 5-pOH-DP to investigate if the interactions were established already in solution. The concentration range of HS-derivatives was selected in relation to their solubility in AN/0.05 M TBAP, as Acetyl-HS was soluble to about 3.5 mM and Cbz-HS was soluble to about 30 mM. Table 3 reports the Epa and j_a data of the dipyrromethanes' oxidation when in solution with and without templates.

The shift to a more anodic value of Epa for both monomers when HS-derivatives were added confirmed that interactions were developed. 5-ph-DP showed a lower interaction efficiency with both templates and the potential shifted just a few mV when either Cbz-HS or Acetyl-HS were added to the solution in equimolar concentrations as the monomer. Moreover, the slight differences of current density j_a ($A \cdot cm^{-2}$) were in the range of experimental reproducibility. However, it was observed that the interactions between 5-pOH-DP and the HS-derivatives made a significant Ep displacement to more positive values (average +50 mV). This is an indication of the complex assembly between the phenol derivative monomer and templates, with Acetly-HS able to pair more efficiently through a hydrogen bonding system than Cbz-HS, in agreement with the NMR data. The value j_a increased by 20% (5.15×10^{-4} $A \cdot cm^{-2}$) when Cbz-HS was added to the monomer solution and it was two times higher with Acetyl-HS (9.39×10^{-4} $A \cdot cm^{-2}$). Zotti et al. [34] observed different ranges of current variations in 2,2′-bypyrrole oxidation when performed in the presence of anions with different electron-donor properties and ion-pairing abilities, suggestive of hydrogen bond formation. The authors considered those effects a consequence of the charge shielding of the radical cation of bipyrrole. Our NMR data showed that the phenol-substituent held in place the non-ionic HS derivatives more than the phenyl-substituent through hydrogen bonding, thus the variation of the current density suggests that a mechanism charge/dipole contributes to the template coordination to the monomer.

Table 3. Epa and j_a variation of the first oxidation process of dipyrromethanes in solutions with templates.

Monomer *	HS-Derivative	Ep_a/mV	j_a/A·cm^{-2}
5-ph-DP	/	873	8.42×10^{-4} (cv % 4.5; n = 5)
5-ph-DP	Cbz-HS (1 mM)	876	7.86×10^{-4} (cv % 3.5; n = 3)
	Cbz-HS (3 mM)	874	6.84×10^{-4} (cv % 5.3; n = 3)
	Cbz-HS (6 mM)	874	6.67×10^{-6} (cv % 5.1; n = 3)
5-ph-DP	Acetyl-HS (1 mM)	879	9.23×10^{-4} (cv % 5.2; n = 3)
	Acetyl-HS (3 mM)	876	6.48×10^{-4} (cv % 5.2; n = 3)
	Acetyl-HS (6 mM)	876	6.22×10^{-4} (cv % 8.5; n = 3)
5-pOH-DP	/	810	4.36×10^{-4} (cv % 5.5; n = 5)
5-pOH-DP	Cbz-HS (1 mM)	850	5.15×10^{-4} (cv % 2.5; n = 3)
	Cbz-HS (3 mM)	870	6.33×10^{-4} (cv % 4.5; n = 3)
	Cbz-HS (6 mM)	850	5.51×10^{-6} (cv % 3.9; n = 3)
5-pOH-DP	Acetyl-HS (1 mM)	889	9.39×10^{-4} (cv % 3.2; n = 3)
	Aceyl-HS (3 mM)	855	6.38×10^{-4} (cv % 5.5; n = 3)
	Acetyl-HS (6 mM)	855	6.63×10^{-4} (cv % 7.5; n = 3)

* 1 mM concentration in AN + 0.05 M TBAP; WE: Pt-quartz crystal electrode vs. Ag/Ag^+ RE and Pt-wire AE; scan rate 50 mVs^{-1}; cv % = coefficient of variation, n = number of measurements.

This consideration holds true for a monomer/template ratio of 1:1 in all investigated blends (also considering the experimental precision measured). Moreover, it was possible to observe a trend of current attenuation when the template concentration increased vs. the constant monomer concentration in solution. It is believed that this result could be due to the different ratio template to monomer, which is responsible for generating complexes with different stoichiometry and different diffusion coefficients [35].

3.3. Electromicrogravimetric (EQCM) Preparation of cNIP and cMIP

The electropolymerization ability of 5-ph-DP was already investigated by EQCM measurements, in which both the cyclic voltammetry and frequency shift due to the mass deposition at the quartz crystal were recorded in parallel [21]. A conductive non imprinted polymer (cNIP) of 5-ph-DP was prepared by cycling the potential between −0.8 V and +1.2 V (vs. Ag/Ag^+) at a scan rate of 50 $mV{\cdot}s^{-1}$. A mass of 1.11×10^{-5} $g{\cdot}cm^{-2}$ (4.99×10^{-8} $mol{\cdot}cm^{-2}$) was obtained at the Pt-quartz crystal electrode (In Supplementary Materials, Figure S2A). The EQCM technique was adopted to assess the ability of 5-pOH-DP to form the polymer as well (In Supplementary Materials, Figure S2B). A mass of 1.7×10^{-5} $g{\cdot}cm^{-2}$ of poly-5-pOH-DP was obtained. In the first cycle, the oxidation peak at about +0.8 V (Figure 2) is assigned to the oxidation of the dipyrromethane unit to its radical cation. The coupling of the radicals and the film formation was confirmed during the second (and subsequent) cycle as a broad anodic peak grown at about +0.2 V due to the oxidation of the formed film of poly-5-pOH-DP. The increase of the current density at both oxidation potentials (+0.8 V and +0.2 V) with the number of cycles is an indication of the electropolymerization process, which was confirmed through the mass increase measured as the frequency shift (In Supplementary Materials, Figure S2A,B and inserts). However, a progressive decrease of the net increment of mass per sweep during deposition was observed. According to the literature, several reasons could explain the observed behavior, as a modification of diffusion of the electroactive species to/from the electrode surface or the intervention of steric hindrance [35–38]. Oligomeric species that are not electrically conductive are reported to be formed during polymerization and these were either embedded into the film with consequent alteration of its uniformity and conductivity and/or they were involved in side reactions of termination that shuttled the radical cations responsible for the polymerization process [39,40]. It is believed that the functional groups in C5 of dipyrromethanes may introduce steric hindrance responsible for structural deformation, which was interfering with the charge transfer process and consequently with the film growth. In consideration of this evidence, we observed that the deposition was efficient up to 12 sweeps which were therefore adopted in the experiments. To prepare the conductive imprinted polymer (cMIP), the electromicrogravimetric deposition of either 5-ph-DP or 5-pOH-DP, was carried out in the presence of a controlled amount of either Acetyl-HS (In Supplementary Materials, Figure S2A,B and inserts) or Cbz-HS. The difference between the total mass deposited at the 12th sweep during the cMIP preparation with those measured at the 12th sweep in the cNIP preparation was used to calculate the formal mass of the template embedded into the film [41]. The Acetyl-HS inclusion into poly-5-ph-DP produced a slight shift (at +0.3 V) in the oxidation of the film. Table 4 compares Δf (Hz) measured at each sweep during cNIP and cMIP deposition by CV (see also in Supplementary Materials, Figure S3). The frequency shift highlights that during cycling, Acetyl-HS was hosted into the film, as the total formal mass deposited increased with respect to that of cNIP, even if a regular deposition was not observed. During CV deposition, in fact, sweeps with negative mass values (meaning that the polymerization behavior of cMIP and cNIP were different) were also observed. A more defined trend of template inclusion was observed when poly-5-ph-DP was templated with Cbz-HS, as the film oxidation shifted about +150 mV (at +0.35 V) and the mass increased with sweep numbers vs. cNIP. The same deposition procedure was adopted with 5-pOH-DP, which was electropolymerized in the presence of the Acetyl-HS template first and, in a second measurement set, with Cbz-HS. In the presence of Acetyl-HS, the phenol-derivative film oxidation shifted to a more positive potential (at +0.4 V), the current intensity increased, and the frequency shift variation confirmed a higher mass was deposited compared to that measured for cNIP (Table 4). Cbz-HS was hosted as well in the poly-5-pOH-DP film, even if at a lower amount. The EQCM data were analyzed in consideration of the NMR data of $\Delta\delta$ and $\Delta\delta/\Delta T$ and a good coherence was observed. As determined by NMR, the interactions between the templates and the 5-ph-DP monomer in solution were very poor (Cbz-HS interacted more than Acetyl-HS), so their lower uptake was explained as being due to the difficulty of holding the template in place by the monomer during polymerization. It is worth noting that the classical anodic electrochemical mechanism of conducting polymer formation involves a “doping” process due to ion

exchange driven by the redox reactions in the polymer matrix (i.e., electrogenerated radical cation and its discharge as a function of the applied potential at the electrode surface) [42]. It is argued that this ion-exchange heterogeneous equilibrium, electrochemically driven, was able to interfere with weaker interactions as it was apparently less evident during 5-pOH-DP polymerization and its cMIP formation. 5-pOH-DP was able to H-bond at phenolic-OH with templates and its uptake ability was more pronounced so that a regular deposition was observed. The less bulky molecule Acetyl-HS (compared to Cbz-HS) tightly interacted with the monomer and it was hosted into the film in higher amounts, as Cbz-HS introduced higher steric hindrance which was detrimental for its uptake.

The increase of the Acetyl-HS binding sites inside the film was evaluated by changing the template concentration with respect to a constant concentration of monomer (1×10^{-3} mol·L^{-1}). It was considered to be advantageous to not increase the film thickness. This would avoid deviation from the Sauerbery equation as a result of alteration of the damping of the frequency oscillation due to the variation of the viscoelastic properties of the film [43]. The formed film was about 100–130 nm thick and was considered rigid, as it was observed that higher film thicknesses were generally required to switch to "rubbery" behavior [43–45]. Moreover, any inclusion has to be quantitatively reversible to avoid "memory effects" and to avoid the need to resort to cleaning that could eventually modify/destroy the structure of the cavity formed into the film [19,20] or delaminate the film from the quartz surface [46].

Table 4. Example of Δf (Hz) measured at each voltage sweep during cNIP and cMIP preparation.

cNIP §	Sweep	Δf/Hz	cMIP §	Sweep	Δf/Hz	Net Δf/Hz*	Δm (ng)
poly-5-ph-DP	1	−303.88	poly-5-ph-DP+ Acetyl-HS	1	−257.25	46.63	−65.28
				2	−327.36	23.28	−32.59
	2	−350.64		3	−346.80	23.28	−32.59
				4	−346.8	30.96	−43.34
	3	−370.08		5	−338.88	−11.52	16.13
				6	−307.68	−46.56	65.18
	4	−377.76	poly-5-ph-DP+ Cbz-HS	1	−257.3	46.6	−65.24
				2	−322.64	28	−39.20
	5	−327.36		3	−342.96	27.1	−37.97
				4	−343.0	34.8	−48.72
	6	−261.12		5	−364.4	−37.04	51.86
				6	−307.68	−46.56	65.18
poly-5-pOH-DP	1	−364.5	poly-5-pOH-DP+ Acetyl-HS	1	−486.80	−112.1	171.74
				2	−512.4	−112.4	157.36
	2	−400.0		3	−532.8	−117.12	163.97
				4	−520.0	−109.44	153.22
	3	−415.7		5	−528.8	−108	151.2
				6	−344.0	71.36	−99.96
	4	−410.6	poly-5-pOH-DP+ Cbz-HS	1	−408.8	−44.3	62.02
				2	−454.8	−54.8	76.72
	5	−420.8		3	−460.8	−45.12	63.16
				4	−467.6	−57.04	79.86
	6	−415.4		5	−474	−53.2	74.48
				6	−468	−52.64	73.65

§ Data refers to 1 mM concentration in solution of both the monomer and template. * Net Δf/Hz = ΔfcMIP − ΔfcNIP. WE: Pt-quartz crystal WE, RE: Ag/Ag$^+$, AE: Pt-wire, scan rate 50 mVs^{-1}, AN/0.05 M TBAP.

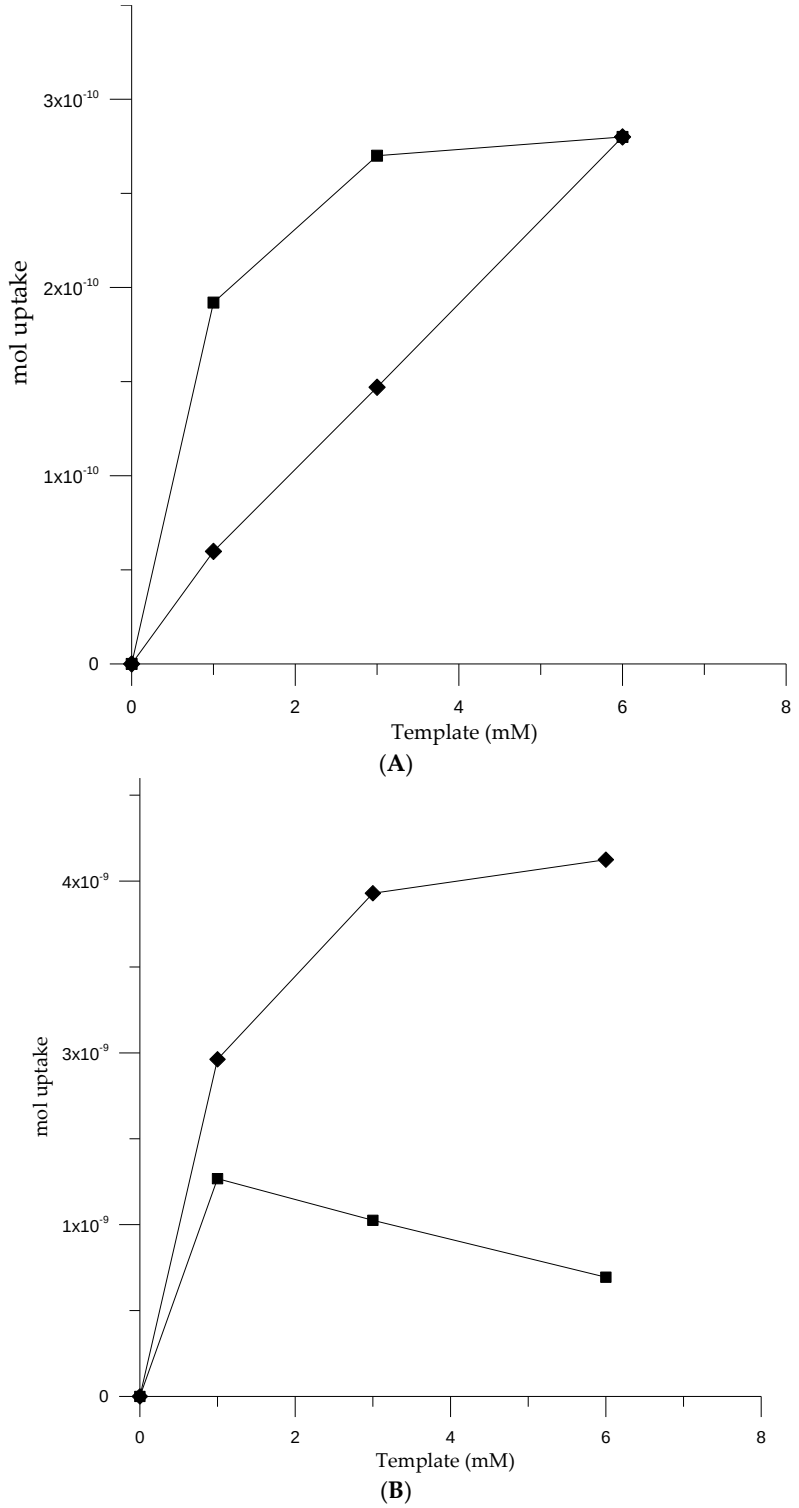

Figure 4. (**A**) Templates hosted by poly-5-ph-DP. Monomer 1 mM in AN + 0.05 M TBAP; WE: Pt-quartz crystal electrode vs. Ag/Ag^+ RE and Pt-wire AE; scan rate 50 mVs^{-1}; (**B**) Templates hosted by poly-5-pOH-DP. Monomer 1 mM in AN + 0.05 M TBAP; WE: Pt-quartz crystal electrode vs. Ag/Ag^+ RE and Pt-wire AE; scan rate 50 mVs^{-1}.

In Figure 4A, the result of template inclusion is expressed as moles of template hosted during film formation at the Pt-quartz crystal (calculated as: moles of cMIP—moles of cNIP for each monomer) as a function of the different concentrations in solution of the template. The formal mole values

were determined by applying the Saurebrey equation (see *Material and Methods*) on the basis of the total measured frequency variation at the 12th sweep of deposition. The inclusion of Acetyl-HS was confirmed to be higher in poly-5-pOH-DP by at least one order of magnitude (about 10^{-9} moles hosted into the polymer) with respect to the uptake ability shown by poly-5-ph-DP (about $10^{-11}/10^{-10}$ moles hosted), over the whole range of concentrations investigated. The same result was observed when Cbz-HS was used as the template. In fact, the uptake shown by poly-5-pOH-DP (Figure 4B) was approximately 10 times higher than that of poly-5-ph-DP. When Cbz-HS was 1 mM in solution it was hosted in a stoichiometric amount by poly-5-pOH-DP. Then the template hosted into the film decreased as its concentration in solution increased. The observed effect was considered to be a consequence of the detrimental effect of the bulky Cbz group on the polymerization [17]. This corroborated the higher inclusion observed for the acetyl-derivative, as its lower size was favorable for molecule proximity (a ratio monomer/template = 1.8 was estimated) with no interferences observed during film polymerization (at the adopted condition). The polymerization capacity of 5-ph-DP in the presence of both templates was observed but a trend to saturation was evident with Cbz-HS. In contrast, this plateau was not observed with Acetyl-HS (whose range of concentration was, however, limited by its solubility in AN/electrolyte).

3.4. Analytical Performances of QCM Sensor cMIPs Modified

To optimize the extraction of the template molecule, a chemical approach was investigated and three solutions of different composition were tested, (i) AN + 0.05 mol·L^{-1} TBAP + 1% (v/v) HAc; (ii) AN + 0.05 mol·L^{-1} TBAP + 10% (v/v) HAc; (iii) AN + 1% (v/v) HAc + 40% (v/v) methanol. The extraction was performed as reported in *Materials and Methods*. A solution with methanol added was initially tested, but a slow drift was always measured and just 13% of the embedded amount of template was extracted in 1 h. Moreover, methanol was found to interact with the polymer structure which imposed a further cleaning step. Washing solutions added with acetic acid offered positive results. Acetyl-HS was extracted from cMIP prepared with both dipyrromethane derivatives in about 15 min when HAc 10% was used. A lower percentage of HAc required a longer time (35 min), as a longer time was always required to extract Cbz-HS. This time ranged from 30 min to 1 h with no significant differences between the two percentages of HAc (either 1% or 10%). Therefore, 45 min with 10% HAc in AN/0.05M TBAP were the conditions adopted to clean cMIPs (92% yield of extraction) followed by an equilibration step of 15 min in AN/0.05M TBAP before the rebinding test was performed. Because it was believed that the polymerization of cMIPs and cNIP could not proceed in the same way, as reported previously in other MIP preparation approaches [47], a rebinding test was performed [21,48] to confirm that the imprinted polymer was obtained.

The 3D-structure of the cavity within the polymeric network was able to selectively rebind HS-derivatives added in the solution as analytes. A typical trend of the frequency shift observed during the rebinding studies on cMIP is reported in Figure S4. The addition of different concentrations of Acetyl-HS to cMIP prepared from a phenol-derivative produced an immediate variation of the crystal oscillation frequency and the response time evaluated at 90% of the signal level was roughly 50 s (the same response time was recorded for the Cbz-HS analyte). The rebinding ability of both cMIPs, prepared with 5-pOH-DP either with Acetyl-HS or Cbz-HS as templates, confirmed that the conditions adopted in their preparation were efficient. The typical trend observed for the rebinding test is reported in Figure 5 as Δf (Hz) vs. the concentration of the homoserine lactone derivative (mol·L^{-1}) added in solution. Data were also expressed in terms of re-bind moles (y-axis on the right side) calculated from the mass variation measured by QCM due to the different concentrations of the analyte (either Acetyl-HS or Cbz-HS) added in solution. A dynamic range between 10^{-8} mol·L^{-1} and 10^{-6} mol·L^{-1} was observed for both templates (i.e., in Acetyl-HS calibration, Δf (Hz) was in the range -16 Hz ($\pm$4.5 Hz)–280 Hz ($\pm$27 Hz)) and the regression equation for Acetyl-HS (expressed as mass variation by application of the Sauerbrey equation) was y = 4 $\times$ 10^{+8} $\times$ (ng (mol·L^{-1})$^{-1}$) + 8.4; (R^2 = 0.9989) and limit of detection (LOD) (3σ of blank signal) was estimated at 1.2 $\times$ 10^{-10} moles.

In the same range of concentration, the slope of the Cbz-HS calibration curve was $3 \times 10^{+8}$ (ng (mol·L^{-1})$^{-1}$) ($R^2 = 0.9908$) with a LOD of 9.8×10^{-11} moles. The range of concentration was investigated using the same cMIP modified QCM crystal, as every addition was followed by a cleaning step for template extraction. As an example, in the determination of Acetyl-HS at 8.3×10^{-7} mol·L^{-1}, a coefficient of variation of 6.5% (n = 5) was determined, with 7.5% for the Cbz-HS measurements (n = 5) at the same concentration. The rebinding investigation of poly-5-ph-DP gave unreliable results, confirming that a good coordination between the monomer and template is mandatory to obtain an effective imprinted polymer.

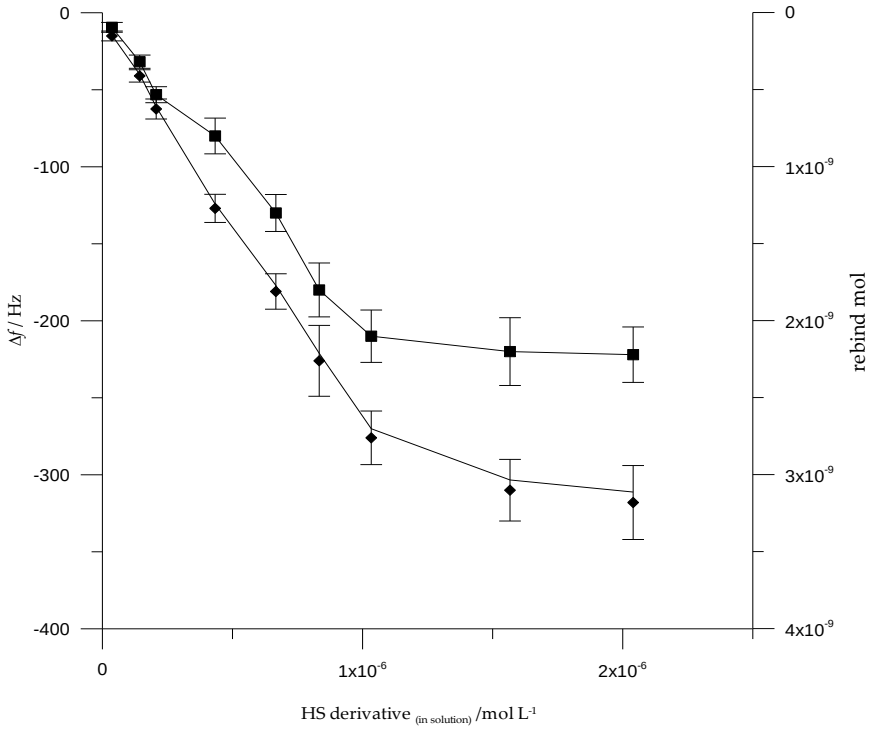

Figure 5. Calibration curves obtained by the rebinding test of cMIP prepared from 1 mM 5-pOH-DP/1 mM Acetyl-HS vs. Acetyl-HS as analyte (diamond symbol), and from 1 mM 5-pOH-DP/1 mM Cbz-HS vs. Cbz-HS as analyte (triangle symbol) in AN + 0.05 M TBAP; WE: Pt-quartz crystal electrode vs. Ag/Ag$^+$ RE and Pt-wire AE; scan rate 50 mVs^{-1}.

3.5. Selectivity Assessment

As interferents, the HS derivative (which was not used as a template in the cMIP preparation), and α-acetylbutyrolactone were tested (Figure 6). It is worth noting that the sensor templated with Acetyl-HS (Figure 6A) showed a very high selectivity, as it essentially recognized itself. Neither Cbz-HS nor α-acetylbutyrolactone were able to be lodged into the Acetyl-HS "fingerprint" obtained for the poly-5-pOH-DP film. In contrast, when Cbz-HS was the template (Figure 6B), the stereo-structure and the shape of the 3D cavity showed a less pronounced selectivity. Thus, rebinding was measured for all three molecules. The uptake of moles of interferent was normalized to the moles of analyte embedded into the film and was expressed as a percentage; 89% was found to be the interfering effect of Acetyl-HS vs. Cbz-HS templated cMIP and 67% was that of α-acetylbutyrolactone vs. Cbz-HS templated cMIP. The main difference characterizing cMIP prepared with these two templates was represented by the presence of different extents of H bonding. Phenolic-OH in 5-pOH-DP was more tightly bound to -NH of Acetyl-HS than -NH of Cbz-HS during polymerization, probably due to their different steric hindrances. This determined a template-monomer arrangement, during polymerization, which imparted a high degree of fitting to the 3D pocket formed around Acetyl-HS. This organization

was necessarily different with Cbz-HS, so that, probably due to steric reasons, it would impose around itself a less "compact" organization during monomer polymerization. It is interesting to note, however, that the recognition pocket obtained was successfully made active not just because its shape was highly compatible with that of the analyte but also because it appeared to require a chemical complementarity. In fact, the chemical structure of α-acetylbutyrolactone lacks a NH-group compared to that of Acetyl-HS. In our opinion, this further confirms the fundamental role of the C5 substituent of dipyrromethane in modulating the selectivity of cMIP, through non-covalent interactions that maintain the template close to the monomer during the polymer growth.

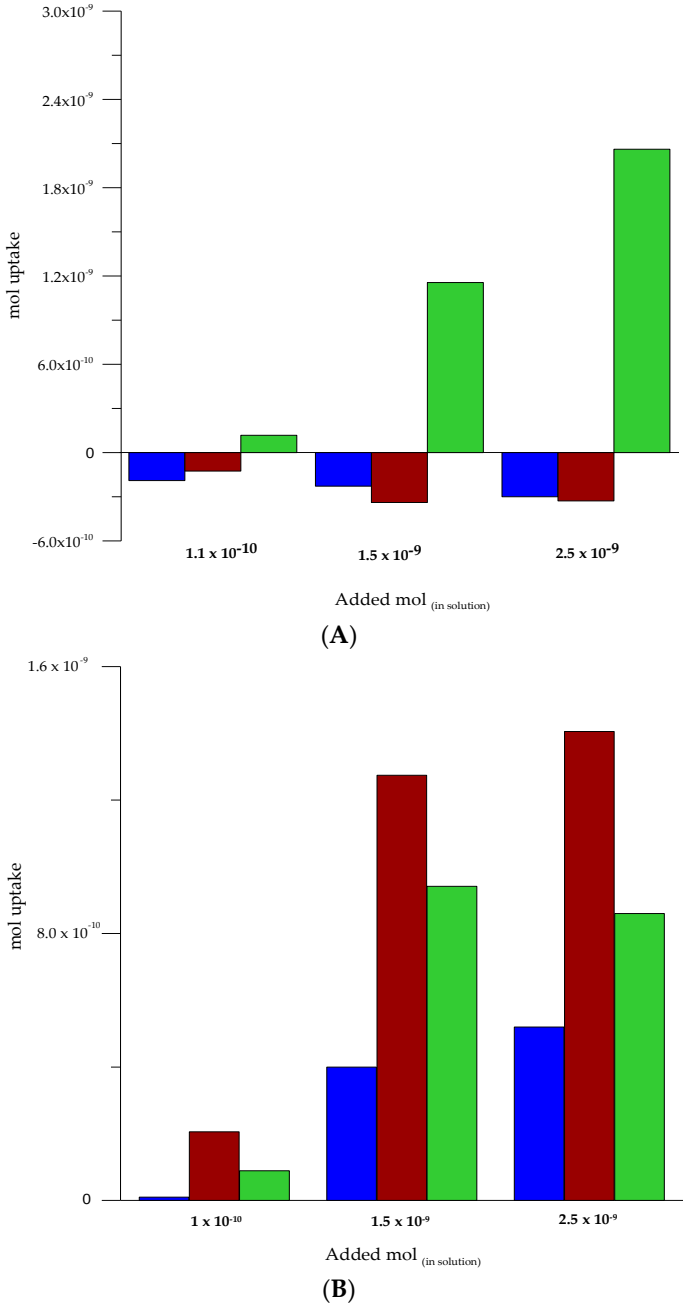

Figure 6. (**A**) cMIP from 5-pOH-DP/Acetyl-HS. Rebinding test vs. Acetyl-HS (red bar) and selectivity assessment vs. Cbz-HS (blue bar) and α-acetylbutyrolactone (green bar); (**B**) cMIP from 5-pOH-DP/Cbz-HS. Rebinding test vs. Cbz-HS (blue bar) and selectivity assessment vs. Acetyl-HS (red bar) and α-acetylbutyrolactone (green bar).

4. Conclusions

This study has demonstrated that the substitution in C5 of dipyrromethanes is a crucial factor in determining the uptake capacity and the selectivity of synthetized cMIP. NMR studies were conducted to better understand how the monomers are arranged around the template prior to polymerization, as the structure and the selectivity of the cMIP cavity depends upon this organization. These data show that 5-pOH-DP was able to assemble to acetyl-homoserine lactone, establishing a detectable H bonding network via the phenolic-OH. On the other hand, 5-ph-DP interacted weakly with the template. The NMR data correlated with the electrochemical measurements and the cMIP prepared with the two monomers confirmed the higher hosting capacity of poly-5-pOH-DP which was at the same time characterized by a high chemical complementarity. These differences in uptake ability between the two dipyrromethanes suggest that dipyrromethanes can act as amino acid-like structures, and that when properly mixed, can help to obtain a synthetic bio inspired pocket.

Supplementary Materials: The following are available online at www.mdpi.com/2227-9040/5/1/5/s1.

Author Contributions: S.S. and C.C. conceived and designed the experiments; S.S. performed the electrochemical and microgravimetric experiments; C.C. performed the organic synthesis, NMR and FTIR characterization and studies; S.S. and C.C. analyzed the data; S.S. and C.C. contributed reagents/materials/analysis tools; S.S. and C.C. wrote the paper.

Conflicts of Interest: The authors declare no conflict of interest.

References

1. Lattach, Y.; Archirel, P.; Remita, S. Influence of the Chemical Functionalities of a Molecularly Imprinted Conducting Polymer on Its Sensing Properties: Electrochemical Measurements and Semiempirical DFT Calculations. *J. Phys. Chem. B* **2012**, *116*, 1467–1481. [CrossRef] [PubMed]
2. Özcan, L.; Şahyn, Y. Determination of paracetamol based on electropolymerized-molecularly imprinted polypyrrole modified pencil graphite electrode. *Sens. Actuators B Chem.* **2007**, *127*, 362–369. [CrossRef]
3. EL-Sharifa, H.F.; Aizawab, H.; Reddy, S.M. Spectroscopic and quartz crystal microbalance (QCM) characterisation of protein-based MIPs. *Sens. Actuators B Chem.* **2015**, *206*, 239–245. [CrossRef]
4. Guardia, L.; Badia, R.; Diaz-Garcia, M.E. Assessment of molecularly imprinted sol-gel materials for selective room temperature phosphorescence recognition of nafcillin. *J. Chromatogr. B* **2004**, *804*, 247–254.
5. Ye, L.; Haupt, K. Molecularly imprinted polymers as antibody and receptor mimics for assays, sensors and drug discovery. *Anal. Bioanal. Chem.* **2004**, *378*, 1887–1897. [CrossRef] [PubMed]
6. Chen, L.; Wang, X.; Lu, W.; Wu, X.; Li, J. Molecular imprinting: Perspectives and applications. *Chem. Soc. Rev.* **2016**, *45*, 2137–2211. [CrossRef] [PubMed]
7. Garcia, R.; Freitas, A.M. Application of Molecularly Imprinted Polymers for the Analysis of Pesticide Residues in Food—A Highly Selective and Innovative Approach. *Am. J. Anal. Chem.* **2011**, *2*, 16–25. [CrossRef]
8. Poma, A.; Brahmbhatt, H.; Pendergraff, H.M.; Watts, J.K.; Turner, N.W. Generation of Novel Hybrid Aptamer–Molecularly Imprinted Polymeric Nanoparticles. *Adv. Mater.* **2015**, *27*, 750–758. [CrossRef] [PubMed]
9. Poma, A.; Piletsky, S.A.; Whitcombe, M.J. *Plastic Antibodiesin Designing Receptors for the Next Generation of Biosensors*, 2nd ed.; Piletsky, S.A., Whitcombe, M.J., Eds.; Springer: New York, NY, USA, 2012; pp. 105–129.
10. Canfarotta, F.; Poma, A.; Guerreiro, A.; Piletsky, S. Solid-phase synthesis of molecularly imprinted nanoparticles. *Nat. Protoc.* **2016**, *11*, 443–455. [CrossRef] [PubMed]
11. Kong, Y.; Zhao, W.; Yao, S.; Xu, J.; Wang, W.; Chen, Z. Molecularly Imprinted Polypyrrole Prepared by Electrodeposition for the Selective Recognition of Tryptophan Enantiomers. *J. Appl. Polym. Sci.* **2010**, *115*, 1952–1957. [CrossRef]
12. Syritski, V.; Reut, J.; Menaker, A.; Gyurcsányi, R.E.; Öpik, A. Electrosynthesized molecularly imprinted polypyrrole films for enantioselective recognition of L-aspartic acid. *Electrochim. Acta* **2008**, *53*, 2729–2736. [CrossRef]

13. Pietrzyk, A.; Suriyanarayanan, S.; Kutner, W.; Chitta, R.; D'Souza, F. Selective histamine piezoelectric chemosensor using a recognition film of the molecularly imprinted polymer of bis(bithiophene) derivatives. *Anal. Chem.* **2009**, *81*, 2633–2643. [CrossRef] [PubMed]
14. Malitesta, C.; Mazzotta, E.; Picca, R.A.; Poma, A.; Chianella, I.; Piletsky, S.A. MIP sensors—The electrochemical approach. *Anal. Bioanal. Chem.* **2012**, *402*, 1827–1846. [CrossRef] [PubMed]
15. Sharma, P.S.; Pietrzyk-Le, A.; D'Souza, F.; Kutner, W. Electrochemically synthesized polymers in molecular imprinting for chemical sensing. *Anal. Bioanal. Chem.* **2012**, *402*, 3177–3204. [CrossRef] [PubMed]
16. Whitcombe, M.J.; Chianella, I.; Larcombe, L.; Piletsky, S.A.; Noble, J.; Porter, R.; Horgan, A. The rational development of molecularly imprinted polymer-based sensors for protein detection. *Chem. Soc. Rev.* **2011**, *40*, 1547–1571. [CrossRef] [PubMed]
17. Bartlett, P.N.; Chung, L.Y.; Moore, P. Conducting polymer films. Attachment of pyrrole groups to aza-macrocycles and attempted electrochemical polymerisation of the resulting monomers. *Electrochim. Acta* **1990**, *35*, 1051–1055. [CrossRef]
18. Curran, D.; Grimshaw, J.; Perera, S.D. Poly(pyrrole) as a support for electrocatalytic materials. *Chem. Soc. Rev.* **1991**, *20*, 391–404. [CrossRef]
19. Janata, J. *Principles of Chemical Sensors*, 2nd ed.; Springer: New York, NY, USA, 2008; pp. 13–50.
20. Sellergen, B.; Hall, A.J. Synthetic Chemistry in Molecular Imprinting. In *Molecular Imprinting: Principles and Applications of Micro- and Nanostructure Polymers*, 1st ed.; Ye, L., Ed.; Pan Stanford Publishing, CRC Press, Taylor & Francis Group: Boca Raton, FL, USA, 2013; pp. 25–65.
21. Susmel, S.; Comuzzi, C. 5-phenyl-dipyrromethane and 5-(4-pyridyl)-dipyrromethane as modular building blocks for bio-inspired conductive molecularly imprinted polymer (cMIP). An Electrochemical and Piezoelectric investigation. *RSC Adv.* **2015**, *5*, 78379–78388. [CrossRef]
22. Lintz, M.J.; Oinuma, K.I.; Wysoczynski, C.L.; Greenberg, E.P.; Churchill, M.E.A. Crystal structure of QscR, a Pseudomonas aeruginosa quorum sensing signal receptor. *Proc. Natl. Acad. Sci. USA* **2011**, *108*, 15763–15768. [CrossRef] [PubMed]
23. Dias, D.M.; Ciulli, A. NMR approaches in structure-based lead discovery: Recent developments and new frontiers for targeting multi-protein complexes. *Prog. Biophys. Mol. Biol.* **2014**, *116*, 101–112. [CrossRef] [PubMed]
24. Van Geet, A.L. Calibration of methanol nuclear magnetic resonance thermometer at low temperature. *Anal. Chem.* **1970**, *42*, 679–680. [CrossRef]
25. Sauerbrey, G. Verwendung von Schwingquarzen zur Wägung dünner Schichten und zur Mikrowägung. *Z. Phys.* **1959**, *155*, 206–222. (In German) [CrossRef]
26. Ka, J.W.; Lee, C.H. Optimizing the synthesis of 5,10-disubstituted tripyrromethanes. *Tetrahedron Lett.* **2000**, *41*, 4609–4613. [CrossRef]
27. Briñas, R.P.; Brückner, C. Triarylcorroles by Oxidative Coupling of Triaryltetrapyrranes. *Synlett* **2001**, *3*, 442–444.
28. Littler, B.L.; Ciringh, Y.; Lindsey, J.S. Investigation of Conditions Giving Minimal Scrambling in the Synthesis of trans-Porphyrins from Dipyrromethanes and Aldehydes. *J. Org. Chem.* **1999**, *64*, 2864–2872. [CrossRef] [PubMed]
29. Ak, M.; Gancheva, V.; Terlemezyan, L.; Tanyeli, C.; Toppare, L. Synthesis of a dipyrromethane functionalized monomerand optoelectrochromic properties of its polymer. *Eur. Polym. J.* **2008**, *44*, 2567–2573. [CrossRef]
30. Ohnishi, M.; Urry, D.W. Temperature dependence of amide proton chemical shifts: The secondary structures of gramicidin S and valinomycin. *Biochem. Biophys. Res. Commun.* **1969**, *36*, 194–202. [CrossRef]
31. Kopple, K.D.; Ohnishi, M.; Go, A. Conformations of cyclic peptides. III. Cyclopentaglycyltyrosyl and related compounds. *J. Am. Chem. Soc.* **1969**, *91*, 4264–4272. [CrossRef]
32. Merutka, G.; Dyson, H.J.; Wright, P.E. Random coil' ^{1}H chemical shifts obtained as a function of temperature and trifluoroethanol concentration for the peptide series GGXGG. *J. Biomol. NMR* **1995**, *5*, 14–24. [CrossRef] [PubMed]
33. Kontogianni, V.G.; Charisiadis, P.; Primikyri, A.; Pappas, C.G.; Exarchou, V.; Tzakosa, A.G.; Gerothanassis, I.P. Hydrogen bonding probes of phenol-OH groups. *Org. Biomol. Chem.* **2013**, *11*, 1013–1025. [CrossRef] [PubMed]

34. Zotti, G.; Schiavon, G.; Zecchin, S.; Sannicolo, F.; Brenna, E. Anion Assisted Anodic Coupling of 2,2′-Bipyrrole. Role of Tosylate Anion in the Electrochemical Synthesis of Polypyrrole. *Chem. Mater.* **1995**, *7*, 1464–1468. [CrossRef]
35. Zheng, W.; Razal, J.M.; Spinks, G.M.; Truong, V.T.; Whitten, P.G.; Wallace, G.G. The Role of Unbound Oligomers in the Nucleation and Growth of Electrodeposited Polypyrrole and Method for Preparing High Strength, High Conductivity Films. *Langmuir* **2012**, *28*, 10891–10897. [CrossRef] [PubMed]
36. Martina, S.; Enklemann, V.; Schluter, A.D.; Wegner, G.; Zotti, G.; Zerbi, G. Synthesis and electrochemical and spectroscopical studies of 2.5-pyrrole oligomers and well-defined short-chain poly(2.5-pyrrole). *Synth. Met.* **1993**, *55*, 1096–1101. [CrossRef]
37. Miles, M.J.; Smith, W.T.; Shapiro, J.S. Morphological investigation by atomic force microscopy and light microscopy of electropolymerised polypyrrole films. *Polymer* **2000**, *41*, 3349–3356. [CrossRef]
38. Suarez, M.F.; Compton, R.G. In situ atomic force microscopy study of polypyrrole synthesis and the volume changes induced by oxidation and reduction of the polymer. *J. Electroanal. Chem.* **1999**, *462*, 211–221. [CrossRef]
39. Higghins, S. Conjugated polymers incorporating pendant functional groups-synthesis and characterization. *Chem. Soc. Rev.* **1997**, *26*, 247–257. [CrossRef]
40. Khairunnisa, A.; Liao, W.; Yau, S. Adsorption and Electrochemical Polymerization of Pyrrole on Au(100) Electrodes as Examined by In Situ Scanning Tunneling Microscopy. *J. Phys. Chem. C* **2016**, *120*, 26425–26434. [CrossRef]
41. Ratautaitea, V.; Plausinaitisa, D.; Baleviciutea, I.; Mikoliunaitea, L.; Ramanaviciene, A.; Ramanavicius, A. Characterization of caffeine-imprinted polypyrrole by a quartz crystal microbalance and electrochemical impedance spectroscopy. *Sens. Actuators B* **2015**, *212*, 63–71. [CrossRef]
42. Sadki, S.; Schottland, P.; Brodie, N.; Sabouraud, G. The mechanisms of pyrrole electropolymerization. *Chem. Soc. Rev.* **2000**, *29*, 283–293.
43. Reed, C.E.; Kanazawa, K.K.; Kaufmann, J.H. Physical description of a viscoelastically loaded AT-cut quartz resonator. *J. Appl. Phys.* **1990**, *68*, 1993–2001. [CrossRef]
44. Susmel, S.; Toniolo, R.; Pizzariello, A.; Dossi, N.; Bontempelli, G. A piezoelectric immunosensor based on antibody entrapment within a non-totally rigid polymeric film. *Sens. Actuators B* **2005**, *111*, 331–338. [CrossRef]
45. Nakluaa, W.; Suedeea, R.; Lieberzeit, P.A. Dopaminergic receptor–ligand binding assays based on molecularly imprinted polymers on quartz crystal microbalance sensors. *Biosens. Bioelectron.* **2016**, *81*, 117–124. [CrossRef] [PubMed]
46. Schweiger, B.; Kim, Y.J.; Ulbricht, M. Electropolymerized Molecularly Imprinted Polypyrrole Film for Sensing of Clofibric Acid. *Sensors* **2015**, *15*, 4870–4889. [CrossRef] [PubMed]
47. Oral, E.; Peppas, N.A. Dynamic studies of molecular imprinting polymerizations. *Polymer* **2004**, *45*, 6163–6173. [CrossRef]
48. Kan, X.; Xing, Z.; Zhu, A.; Zhao, Z.; Xu, G.; Li, C.; Zhou, H. Molecularly imprinted polymers based electrochemical sensor for bovine hemoglobin recognition. *Sens. Actuators B* **2012**, *168*, 395–401. [CrossRef]